AI-Assisted Composite ISAC for mmWave Respiration Pattern Recognition

Xiaochan Xue*, Saurabh Parkar*, Shucheng Yu†, Yao Zheng*

*Department of Electrical and Computer Engineering, University of Hawai'i at Mānoa, HI 96822, USA
†Department of Graduate Computer Science and Engineering, Yeshiva University, NY 10033, USA
Email: {xxue,sparkar,yaozheng}@hawaii.edu, shucheng.yu@yu.edu

Abstract—Respiratory monitoring is essential for early detection of various health conditions. Conventional methods rely on contact sensors or clinical equipment, limiting usability for daily healthcare or remote settings. Wireless sensing provides a contactless alternative; however, OFDM-based systems face challenges in resolution and motion robustness, while FMCW radars lack communication capabilities without additional hardware.

In this paper, we make an attempt toward a lightweight Integrated Sensing and Communication (ISAC) system by embedding narrowband FMCW signals into the guard bands of OFDM channels. This re-purposing enables high-resolution sensing and reliable communication simultaneously, without modifying the OFDM structure or introducing extra hardware. We explore trade-offs between sensing accuracy and communication quality, evaluated in terms of Error Vector Magnitude (EVM), under varying FMCW sweep bandwidths and FMCW-to-OFDM power ratios. By integrating signal enhancement techniques and a 1D-CNN classifier, we develop a robust respiratory pattern recognition system resilient to motion interference.

We implement a 28 GHz mmWave testbed with USRPs. Through extensive experimental evaluation, we determine suitable parameter settings for the proposed composite waveform based on EVM performance and alignment with ground truth measurements. Ultimately, our system classifies four respiratory patterns achieves over 98% accuracy, demonstrating its effectiveness and practicality for wireless health monitoring.

Index Terms—Integrated Sensing and Communication (ISAC), mmWave Sensing, Composite OFDM-FMCW Waveform, Channel State Information (CSI), Machine Learning, Respiration Pattern Recognition

I. INTRODUCTION

Respiration is one of the most vital human life activities and plays a critical role in maintaining normal physiological and mental functions. Key respiratory parameters offer valuable insights into an individual's physical and psychological states. Therefore, accurate and timely detection of respiratory disorders is of significant importance.

In the past decades, various respiration detection techniques such as Capnography, Pulse Oximetry, Arterial Blood Gas (ABG) analysis, and lung MRI have been developed. While reliable, these methods depend on specialized equipment and clinical settings, limiting their use in daily or remote environments. To improve accessibility, portable solutions have emerged. For instance, Respiratory Inductive Plethysmography (RIP) [1] uses chest and abdominal bands for ambulatory monitoring. Vision-based contactless approaches [2, 3] using RGB or infrared cameras have also been explored, but suffer from sensitivity to lighting, occlusion, and privacy issues.

The rise of smart homes and telehealth services has created demand for unobtrusive health monitoring systems that seamlessly integrate into daily life. An ideal solution would leverage existing wireless infrastructure (e.g., 5G small cells or home gateways) to provide continuous respiration monitoring without dedicated sensors or cameras. This approach offers several advantages: no additional hardware deployment, privacy preservation, and the ability to reuse underutilized spectrum resources for health sensing. *Integrated Sensing and Communication (ISAC)* serves as a design paradigm in which sensing and communication coexist on shared hardware, spectrum, and control [4].

Realizing ISAC for respiration monitoring depends critically on waveform and processing choices. Wireless signals can be repurposed for contactless breathing detection, but existing approaches exhibit complementary limitations. *Orthogonal Frequency-Division Multiplexing (OFDM)-based systems* estimate respiration from Channel State Information (CSI) [5–7]. mmWave CSI methods further exploit Doppler with learning and reference channel cancellation [8]. However, limited range resolution and strong multipath dependence thwart motion robustness and fine-grained spatial localization.

In contrast, *Frequency Modulated Continuous Wave (FMCW)-based systems* offer centimeter-level range resolution and high sensitivity to micro-motions (e.g., chest displacement), with reliable respiration and heart-rate detection at 77 GHz in LoS and NLoS settings [9, 11, 12]. But standalone FMCW lacks built-in communication capabilities. Using a separate system increases both the cost and the use of the spectrum, which is against the ISAC goal of resource sharing.

Therefore a central challenge is to design waveforms that serve communication and sensing simultaneously with acceptable performance in both. *Composite waveform* has emerged as a promising approach to address this challenge. The core idea is to combine multiple signal types (e.g., OFDM for communication and FMCW for sensing) within one transmission to exploit complementary strengths. Prior work [13–15] explores chirp embedding, non-orthogonal superposition, and time-multiplexing, aiming to keep OFDM data rates while preserving FMCW resolution. However, these designs face practical barriers. Most of existing works require complex modulation, precise timing and phase alignment, or sophisticated interference cancellation, which adds implementation overhead. This challenge is especially severe in mmWave 5G

Table I
COMPARATIVE ANALYSIS

REF.	SIGNAL TYPE	PROCESSING	INTERFERENCE	DETECTION	CLASSIFIER	ACCURACY
Kontou et al. [7]	WiFi 802.11ac (5GHz)	Hampel Filter, PCA	No Interference	Respiration Rate	ANN	98.6%
Wu et al. [8]	OFDM, Radar (60.48GHz)	CAF, 2D-CFAR	External Person Interference	Presence and Respiration Rate	ResNet	90%
Hao et al. [9]	FMCW (77GHz)	Signal overlay, HOG	Background Interference	Respiration Patterns	G-SVM	94.75%
Luo et al. [10]	OFDM (28GHz)	Smoothing, EWT	No Interference	Respiration Rate	FFT	94%
Our Work	OFDM, FMCW (28GHz)	Smoothing, EWT, Normalization	Moderate Body and Hand Movement	Respiration Patterns	1D-CNN	98.5%

(e.g., Band n257: 26.5–29.5 GHz), where spectrum is limited and shared with high-throughput services. More critically, the practical feasibility of composite OFDM–FMCW waveforms remains largely unvalidated on real hardware. Without empirical evidence, it is unclear whether they can move from theory to deployable ISAC systems.

In this work, we present an OFDM–FMCW composite ISAC system at 28 GHz (5G NR mmWave). We embed a narrowband FMCW signal in the OFDM guard band, avoiding structural changes to OFDM and minimizing overlap. This enables simultaneous high-resolution sensing and communication without additional hardware. Because guard-band reuse can introduce interference to adjacent subcarriers, we quantify its impact under varying sweep bandwidth (0.25–2 MHz) and FMCW-to-OFDM power ratio (0.1–2). Using EVM and ground-truth alignment as metrics, our experiments characterize the trade-offs between sensing and QoS and show that a usable data link and accurate sensing can coexist. We validate the system on a 28 GHz mmWave testbed with USRP radios and phased-array antennas. Our main contributions are summarized as follows:

- We propose a lightweight composite ISAC waveform that embeds narrowband FMCW in OFDM guard bands at 28 GHz, enabling simultaneous communication and respiration sensing without restructuring OFDM.
- We extensively evaluate FMCW-induced interference across parameters and provide baselines for choosing practical sensing–communication trade-offs.
- We implement and validate the system on a real mmWave testbed with USRPs and phased arrays, demonstrating superior FMCW sensing over CSI-based methods in ground-truth alignment.
- Our end-to-end signal processing and classification pipeline achieves over 98% accuracy on four respiratory patterns, confirming the practicality of the design.

The remainder of this paper is organized as follows. Section II reviews related work. Section III introduces technical background. The composite waveform detection system is presented in Section IV, followed by experimental results in Section V. We conclude the paper in Section VI.

II. RELATED WORK

This section reviews wireless respiration sensing in three categories: OFDM-based methods, FMCW-based methods, and composite signals. Table I summarizes representative prior work and contrasts it with our approach, highlighting differences in waveform design, processing, and performance.

OFDM-Based Respiration Sensing. OFDM-based systems leverage CSI from existing wireless communication infrastructure to detect respiratory patterns. Liu et al. [5] utilized CSI data from Wi-Fi access point pairs to monitor respiration rates during sleep, demonstrating the feasibility of using communication signals for vital sign monitoring. Wang et al. [6] employed Wi-Fi (802.11n) at 5.24 GHz with 30 OFDM subcarriers, applying Hampel and Moving Average filters for denoising, followed by variance-based subcarrier selection. Their system successfully distinguished individual frequency variations through Power Spectral Density (PSD) analysis.

Kontou et al. [7] proposed a Wi-Fi-based system using 802.11ac at 5 GHz to estimate respiratory rate from CSI amplitude. Their preprocessing involved Hampel filtering and Principal Component Analysis (PCA), with an Artificial Neural Network (ANN) model achieving 98.6% accuracy, though limited to static conditions. Recent mmWave advances include Wu et al. [8], who presented a 60.48 GHz OFDM-based system using Doppler processing with Cross Ambiguity Function (CAF) and 2D Constant False Alarm Rate (CFAR) algorithms, achieving 90% accuracy with ResNet classification. Luo et al. [10] implemented an OFDM system at 28 GHz using smoothing and Empirical Wavelet Transform (EWT), achieving 94% accuracy through FFT-based analysis.

Despite these advances, OFDM-based approaches face fundamental limitations including limited range resolution, ambiguity in target localization due to multipath propagation, and sensitivity to frequency-selective fading.

FMCW-Based Respiration Sensing. FMCW radar systems demonstrate superior performance in vital sign detection due to excellent range resolution and high sensitivity to small-scale motions. Alizadeh et al. [11] used a 77 GHz FMCW radar with a 3.99 GHz sweep to extract respiration and heart rate, achieving 94% and 80% accuracy. Li et al. [12] demonstrated non-line-of-sight operation with an 896 MHz sweep for simultaneous vital-sign monitoring and human localization. Hao et al. [9] implemented a 77 GHz FMCW system with a 4 GHz sweep for respiration-pattern detection, applying signal superimposition for static-noise suppression and HOG features, achieving 94.75% with a Gaussian SVM.

However, FMCW-based systems present significant limitations for integrated applications. Traditional FMCW radars lack inherent communication capabilities, requiring separate communication systems that increase hardware complexity

and reduce spectrum efficiency. Their relatively low spectral efficiency compared to modern communication waveforms makes them unsuitable for high-data-rate applications.

Composite Signal Approaches. Recent research has explored composite waveforms that combine multiple signal types to leverage complementary sensing and communication capabilities. Bouziane et al. [13] proposed a DFT matrix-based method that embeds chirp components into a custom modulator, enabling analog-domain radar processing while maintaining communication performance. Jia et al. [14] introduced frequency-domain OFDM-chirp waveforms by applying chirp-modulated phases to OFDM subcarriers, improving Doppler robustness but requiring precise chirp phase alignment. Mert Şahin and Arslan [15] demonstrated non-orthogonal superposition of FMCW and OFDM signals over the same bandwidth, achieving joint sensing and data transmission but at the cost of complex waveform coordination and interference cancellation. While effective, these methods often require additional processing or structural changes. In contrast, our approach embeds a narrowband FMCW signal into the OFDM guard band, enabling joint sensing and communication without modifying the waveform or increasing complexity.
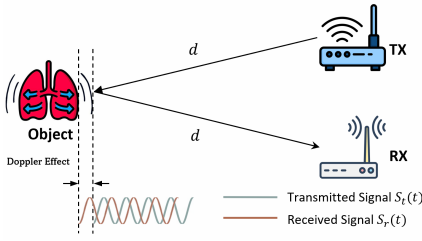

Figure 1. The signal emitted from TX towards a subject exhibiting the Doppler effect, and reflected back to RX.

III. PRELIMINARIES

A transmitted signal reflects off a subject and returns with Doppler Effect due to chest motion, as shown in Fig. 1. For OFDM-based sensing, these variations manifest across the CSI of subcarriers, whereas in FMCW radar signals, they appear as small frequency shifts in the received signal, observable in the beat signals for subsequent analysis.

A. OFDM

Orthogonal Frequency-Division Multiplexing (OFDM) is the fundamental modulation scheme employed in 5G NR communication systems. It provides high spectral efficiency, robustness against multipath fading, and fine-grained frequency-domain resource allocation, making it well-suited for both data transmission and integrated sensing applications.

An OFDM signal is composed of multiple orthogonal subcarriers, each modulated by a complex symbol. The baseband OFDM signal $S_t(t)$ with N subcarriers is:

$$S_t(t) = \sum_{n=0}^{N-1} X_n e^{j2\pi f_n t}, \quad 0 \leq t \leq T \tag{1}$$

where X_n is the complex symbol transmitted on the n-th subcarrier, $f_n = f_0 + n\Delta f$ is the subcarrier frequency, and $\Delta f = \frac{1}{T}$ is the subcarrier spacing.

In a wireless channel, each subcarrier experiences different amplitude and phase distortions due to multipath propagation and motion-induced Doppler shifts. The received subcarrier at index k and OFDM symbol n is modeled as:

$$S_{r,k}[n] = H_k[n] \cdot X_k[n] + N_k[n] \tag{2}$$

where $H_k[n]$ is the complex channel coefficient (Channel State Information, CSI), and $N_k[n]$ represents the additive noise. The phase component $\phi_k[n] = \arg(H_k[n])$ contains rich temporal information about motion within the environment.

B. FMCW Radar

Frequency Modulated Continuous Wave (FMCW) is a radar technique where the frequency of a continuous wave varies linearly over time. A transmitted FMCW signal $S_t(t)$ is sent to the breathing subject and is expressed as:

$$S_t(t) = A\cos(2\pi(f_c t + \frac{B}{2T}t^2)) \tag{3}$$

where A is the amplitude, f_c is the carrier frequency, B is the sweep bandwidth, and T is the chirp duration. The instantaneous transmitted frequency $f_t(t)$ is obtained by calculating the derivative of the phase:

$$f_t(t) = \frac{1}{2\pi}\frac{d}{dt}(2\pi(f_c t + \frac{B}{2T}t^2)) = f_c + \frac{B}{T}t \tag{4}$$

From Eq. (4), we can observe the chirp characteristic, where the frequency changes linearly over time within a fixed range. When reflecting off the subject, the signal experiences a time delay $\tau = \frac{2d}{c}$, where c is the speed of light and $2d$ represents the round-trip traveling path of $S_t(t)$ from transmitter to the subject and reflected back to the receiver. With this time delay, the received signal $S_r(t)$ is given by:

$$S_r(t) = A\cos(2\pi(f_c(t-\tau) + \frac{B}{2T}(t-\tau)^2)) \tag{5}$$

According to Eq. (5), the transmitted signal continues to sweep linearly in frequency throughout the process. The instantaneous received frequency $f_r(t)$ is expressed as:

$$f_r(t) = \frac{1}{2\pi}\frac{d}{dt}\left(2\pi\left(f_c(t-\tau) + \frac{B}{2T}(t-\tau)^2\right)\right)$$
$$= f_c + \frac{B}{T}(t-\tau) \tag{6}$$

Due to the time delay τ during round-trip propagation, the received signal has a lower frequency than the current transmitted signal. The difference defines the beat frequency:

$$f_b = f_t(t) - f_r(t) = \frac{2Bd}{cT} \tag{7}$$

For periodic chest motions due to breathing, a dynamic component f_D caused by the periodic Doppler effect will be added to the beat frequency f_b. The Doppler frequency shift is given by $f_D = \frac{4v_{\max}}{\lambda}\sin(2\pi f_{\text{breath}}t)$, where $v_{\max}$ is the maximum chest velocity, λ is the wavelength, and f_{breath} is the breathing frequency. In this scenario with moving subjects, the modulated beat frequency f_{mb} is given by:

$$f_{\text{mb}} = f_D + \frac{2Bd}{cT} \tag{8}$$

This dynamic modulation causes periodic shifts in the beat frequency due to inhalation and exhalation. By performing Fast Fourier Transform (FFT) on the modulated beat frequency f_{mb}, the static component $\frac{2Bd}{cT}$ appears as a DC offset (0 Hz component), while the dynamic breathing component f_D produces spectral peaks at the fundamental breathing frequency and its harmonics.

C. Signal-to-Noise Ratio

The Signal-to-Noise Ratio (SNR) quantifies a radar system's ability to separate target echoes from noise and is defined as:

$$\text{SNR} = \frac{P_t G_t G_r \lambda^2 \sigma}{(4\pi)^3 d^4 k T_{\text{sys}} F B_r} \tag{9}$$

The numerator of the SNR equation reflects received signal power, influenced by transmit power P_t, antenna gains G_t and G_r, wavelength λ, radar cross-section σ, and target distance d. The denominator represents noise power, determined by Boltzmann's constant k, system noise temperature T_{sys}, receiver noise figure F, and bandwidth B_r.

Since noise power scales linearly with B_r, reducing receiver bandwidth improves SNR. However, range resolution degrades with narrower sweep bandwidth B, following $\Delta R = c/(2B)$. To avoid aliasing, B must remain within the receiver bandwidth and is typically constrained by $B < B_r/2$. In 5G NR-based radar systems, where bandwidths typically range from 10^6 to 10^8 Hz, balancing SNR and resolution is critical. Although lower sweep bandwidths increase SNR, they also reduce range resolution and signal energy per chirp, impairing detection of fine patterns such as breathing. To compensate, higher transmit power or antenna gain is required, at the cost of increased power consumption, which must be considered in energy-constrained scenarios.

D. Breathing Patterns

Abnormal breathing patterns often indicate underlying physiological or pathological conditions. This study focuses on four representative patterns: Eupnea, Bradypnea, Kussmaul, and Biot's respiration [16]. Eupnea refers to normal, smooth, and rhythmic breathing. Bradypnea is characterized by abnormally slow rate, often linked to hypoventilation from drug overdose, brainstem injury, or metabolic disorders. Kussmaul breathing presents as deep and rapid respiration, typically observed in metabolic acidosis such as diabetic ketoacidosis. Biot's respiration, associated with brainstem damage or elevated intracranial pressure, features irregular breathing interrupted by unpredictable apneic episodes.

Table II
BREATHING PATTERNS DESCRIPTION

No.	PATTERNS	RESPIRATION EFFORT	RESPIRATORY RATE RANGE BREATHS PER MINUTE
1	Bradypnea	1	5-10
2	Eupnea	1	12-25
3	Kussmaul	2.5	20-35
4	Biot's	1	12-25

Two features distinguish breathing types: Respiratory Rate (RR) and Respiratory Effort (RE). RR represents breaths per minute, reflecting ventilation efficiency. RE represents muscular effort for breathing, estimated using biomechanical indicators. As shown in Table II, Eupnea maintains moderate RR with minimal effort, Bradypnea reduces RR at the same effort level, Kussmaul increases RR and effort, while Biot's respiration maintains RR but is disrupted by irregular pauses.

IV. COMPOSITE WAVEFORM DETECTION SYSTEM

A. Composite Signal Generation

To enable integrated sensing and communication, we construct a composite signal by embedding a narrowband FMCW radar signal into the guard band of a 5G NR OFDM waveform. This approach leverages unoccupied spectral resources to maximize resource utilization while maintaining the fundamental OFDM structure. The guard band provides spectral separation between the FMCW component and active OFDM subcarriers, though potential interference effects on communication performance are addressed through careful system design and will be discussed in the evaluation section.

To improve power efficiency while maintaining sensing performance, the FMCW waveform is configured with narrow sweep bandwidth and short chirp durations. As discussed in Section III-C, selecting appropriate chirp lengths and idle intervals reduces average transmit power, enabling low-power operation suitable for continuous health monitoring.

This design avoids extra bandwidth and reduces need for continuous radar transmissions. Compared to traditional FMCW systems, our approach achieves reliable respiration sensing with lower energy consumption and minimal impact on communication performance.

B. Breathing Detection Scheme

With the OFDM-FMCW composite signal designed as described in Section IV-A, the following section details the breathing pattern detection scheme, consisting of the following five steps outlined in Fig. 2.

Step 1: Signal Deployment
The composite signal is transmitted toward the subject via the ISAC system, leveraging spectral separation to support concurrent sensing and communication.

Step 2: Data Collection
The subject simulates the different breathing patterns described in Table II under the following postural conditions: **(i)** static postures with the subject facing different directions, **(ii)** deliberate hand movements, and **(iii)** moderate body movements, including lateral (left–right) and axial (front–back) shifts. These conditions emulate a more realistic subject behavior during respiration monitoring.

Step 3: Data Processing
a. Data Extraction At the receiver, the composite signal is separated into 5G NR OFDM and FMCW components using band-pass filters. These modalities are independently processed to extract respiratory information.
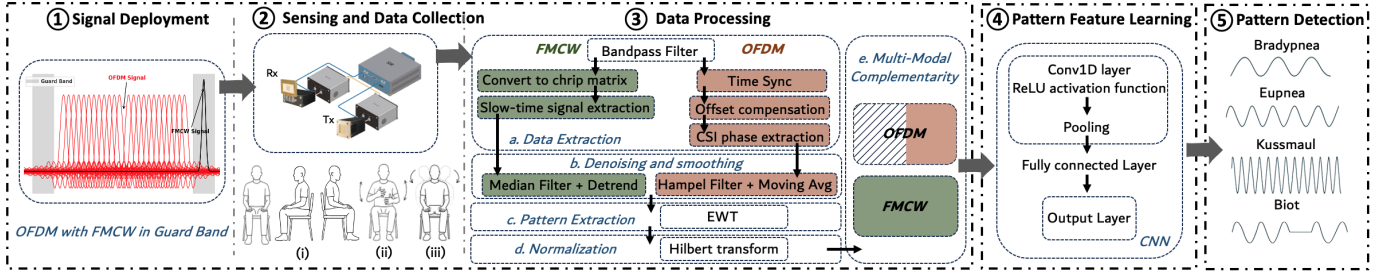
Figure 2. System Overview. **Step 1:** Signal Deployment; **Step 2:** Sensing and Data Collection; **Step 3:** Data Processing; **Step 4:** Artificial-Intelligence-based Pattern Feature Learning; **Step 5:** Breathing Pattern Detection Output.

For the 5G NR component, the filtered signal undergoes time synchronization and frequency offset compensation. CSI is estimated for each active subcarrier, from which the subcarrier-specific phase is extracted. The measured phase for the sth symbol and k^{th} subcarrier is modeled as:

$$\hat{\phi}_{s,k} = \phi_{s,k} + \underbrace{2\pi \frac{m_k}{N} \cdot \Delta t}_{\text{SFO, STO}} + \underbrace{\gamma}_{\text{CFO}} + Z \qquad (10)$$

Here, $\hat{\phi}_{s,k}$ denotes the measured phase and $\phi_{s,k}$ is the true phase. The term $2\pi \frac{m_k}{N} \cdot \Delta t$ captures sample frequency offset (SFO) and sample timing offset (STO) effects, γ accounts for carrier frequency offset (CFO), and Z represents measurement noise. Linear detrending removes phase distortion introduced by SFO and STO [17].

For the FMCW component, the received signal is dechirped into beat signals and reshaped into a chirp matrix. Tracking a specific range bin across successive chirps forms a slow-time signal capturing micro-motion effects. A detrend filter suppresses low-frequency drift and oscillator-induced artifacts.

b. Denoising and Smoothing: Respiratory signals are often corrupted by abrupt phase jumps and movement-induced noise. A multi-stage denoising pipeline is applied: first, a Hampel filter suppresses outliers using Median Absolute Deviation (MAD) as a robust dispersion metric. Next, a moving average filter smooths CSI-phase signals, while a median filter is applied to radar slow-time signals to reduce impulse noise.

c. Pattern Extraction: To isolate respiratory patterns from low-frequency noise, Empirical Wavelet Transform (EWT) is applied to both slow-time and CSI-phase signals. EWT adaptively decomposes each signal into frequency bands, with one band predominantly capturing respiratory activity while others contain residual noise.

d. Normalization: The extracted respiratory signal is converted into an analytic signal using the Hilbert transform to compute a smooth amplitude envelope. This reduces signal variability and highlights the rhythmic structure of breathing, producing a consistent representation suitable for deep learning-based prediction.

e. Multi-Modal Complementarity: Under static conditions, both OFDM and FMCW modalities provide reliable respiratory measurements. However, during dynamic conditions with body movement interference, OFDM-based CSI measurements become susceptible to multipath variations and frequency-selective fading. In these scenarios, FMCW radar plays a crit-

ical role by maintaining high sensitivity to micro-motions and superior range resolution, ensuring robust respiratory detection when OFDM data quality degrades. This complementary behavior enables the system to adapt to varying environmental conditions and movement patterns.

Step 4: Pattern Features Learning The extracted breathing patterns are fed into a 1-D Convolutional Neural Network for classification. The network learns specific pattern features from the extracted breathing waveform to distinguish between different respiratory patterns.

Step 5: Breathing Pattern Detection The individual samples are classified according to the characteristics of each different pattern. Then, breathing patterns are detected successfully.

V. Evaluation

In this section, we experimentally validate the effectiveness of our dual-mode ISAC system, breathing pattern detection, and extraction.
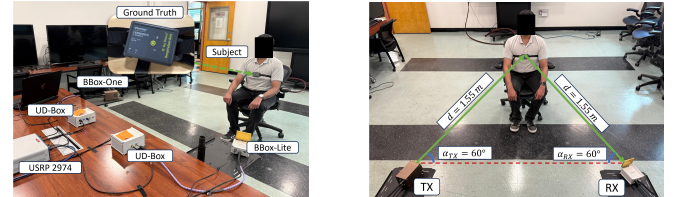

Figure 3. Breathing patterns detection setup. Left: All entities. Right: Specific antennas and subject setup for breathing pattern detection.

Experimental Setup: The mmWave ISAC system uses an NI-USRP 2974 and GNU Radio. Baseband signals at 2.8 GHz are upconverted to 28 GHz via a TMYTEK UD-Box. A 16-channel phased array (BBox-One) transmits and a 4-channel array (BBox-Lite) receives. Arrays use a 30° horizontal aperture, yielding $\alpha_{\text{TX}} = \alpha_{\text{RX}} = 60°$ unde line-of-sight (LoS) conditions. The 5G NR link operates at a 50 MHz sample rate, 40 MHz bandwidth, and 60 kHz subcarrier spacing, using 240 subcarriers over 20 resource blocks. With 16-QAM and a 0.3320 code rate, the system achieves 11.42 Mbps throughput and maintains 14% EVM, as summarized in Table III.

A. FMCW Parameters Selection

The OFDM–FMCW composite system design hinges on selecting appropriate parameters that balance sensing accuracy with communication reliability. In this subsection, we detail the rationale for configuring the FMCW sweep bandwidth and transmit power allocation.

PARAMETERS	VALUES
Channel Bandwidth	40 MHz
Subcarrier Spacing	60 kHz
Resource Blocks	20
Subcarriers	240
Modulation	16 QAM
Target Code Rate	0.3320
Error Vector Magnitude (EVM)	14%
Throughput	11.42 Mbps

FMCW Sweep Bandwidth Selection: Our system transmits a narrowband FMCW signal alongside the 5G NR communication signal, with the FMCW component placed 18 MHz away from the center frequency to minimize interference. To balance sensing performance and spectral efficiency, we evaluate sweep bandwidths ranging from 2 MHz to 0.25 MHz. Each FMCW chirp lasts 1 ms, with a chirp repetition rate of 1 kHz. While narrower sweep bandwidths (e.g., 1 MHz, 0.5 MHz, 0.25 MHz) occupy less spectrum and reduce potential interference, they also degrade range resolution, governed by $\Delta R = \frac{c}{2B}$. To maintain sensing accuracy under narrow bandwidths, higher antenna gains are required—for example, increasing transmit gain (G_t) from 10 dB to 15 dB and receive gain (G_r) from 20 dB to 25 dB. However, this leads to increased power consumption and hardware complexity, as discussed in Section III-C. Considering these trade-offs, we select a 2 MHz sweep bandwidth as the primary configuration for our system.

FMCW Power Allocation: The transmit power of the embedded FMCW component critically affects the trade-off between sensing and communication. As shown in Table IV, when FMCW and OFDM are transmitted with equal power (Ratio = 1), the average EVM increases to 22.65%, representing only an 8% degradation compared to OFDM-only transmissions. Lower FMCW power ratios (0.5, 0.25, 0.1) reduce EVM to around 16–17%, minimizing interference but also lowering the SNR, which weakens chirp returns and reduces robustness under realistic motion and noise conditions. In contrast, higher ratios (≥ 1.25) significantly increase interference, with severe degradation in the first 50 subcarriers and unfeasible EVM values for reliable communication.

Final Configuration: To balance sensing reliability and communication quality, we set a threshold of 50% EVM for evaluating respiration pattern extraction. Based on this guideline, a 2 MHz FMCW sweep bandwidth with transmit power ratios under 1.25 provides sufficient SNR for accurate pattern classification, while keeping communication degradation within acceptable limits for short-range mmWave deployments.

B. Data Collection and Processing

A composite 5G NR–FMCW signal is transmitted toward a single human subject over a 30-second interval, during which the respiratory patterns described in Table II are simulated. Sensing data is collected under three distinct environmental conditions, as outlined in Step 2 of Section IV-B. The received
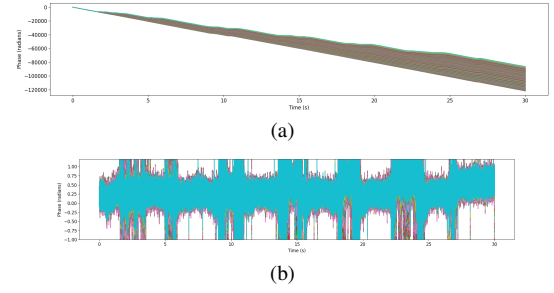

(a)

(b)

Figure 4. Phase sanitization of 5G CSI phase over a 30-second window with six respiratory cycles. (a) Raw phase with SFO/STO trend. (b) Zoomed view showing respiratory cycles amid noise.

Table IV
EVM ANALYSIS FOR FMCW POWER ALLOCATION

	EVM ACROSS FMCW BANDWIDTHS				
	DIFFERENT FMCW SWEEP BANDWIDTH (Hz)				AVERAGE
RATIO	2M	1 M	0.5M	0.25M	–
2	109.94%*	119.64%*	122.96%*	138.56%	**122.77%**
1.75	54.86%*	106%*	111.78%*	128.56%*	**100.3%**
1.5	46.6%	57.98%*	86.44%*	91.73%*	**70.68%**
1.25	37.76%	46.09%*	46.54%*	72.01%*	**50.6%**
1	20.36%	23.91%	24.83%	21.49%	**22.65%**
0.5	16.77%	17.03%	16.88%	17.11%	**16.95%**
0.25	13.49%	17.05%	18.05%	18.16%	**16.91%**
0.1	15.96%	16.11%	16.12%	15.94%	**16.03%**

* The EVM is based on removing the degraded ∼50 first subcarriers.

composite signal is separated into its individual components using bandpass filters centered on the respective spectral regions of the FMCW and 5G NR OFDM modes.

FMCW Slow-Time signal extraction: The beat signal is extracted from the isolated FMCW waveform and reshaped into a chirp matrix. An initial FFT is performed to locate the target's beat frequency peak. With a chirp repetition rate of 1 kHz over 30 seconds, the matrix has dimensions of $30,000 \times 20,000$, where each row is a range profile. This chirp rate offers sufficient temporal resolution to capture respiratory motion while keeping processing manageable. A second FFT is applied row-wise to extract range information, and the range bin corresponding to the target peak is selected to form a slow-time signal of length 30,000. Variations in peak magnitudes over time reflect respiration-induced chest movements.

OFDM CSI-Phase Sanitization: The CSI-phase extraction process for the 5G signal is illustrated in Fig. 4, using a 30-second sample with six respiratory cycles. As shown in Fig. 4a, the raw phase exhibits a downward linear trend from SFO and STO, removed via linear compensation (Fig. 4b). Although residual noise and amplitude variations remain, the respiratory pattern becomes clearer. After sanitization, respiratory rhythms appear consistently across active subcarriers with minimal variance. The subcarrier with the lowest EVM is selected for further processing to ensure reliability.

Following the separation of 5G and FMCW components, their corresponding CSI-phase and slow-time signals are extracted. Both undergo a unified three-stage processing pipeline: (i) smoothing to reduce residual noise, (ii) EWT-based decom-
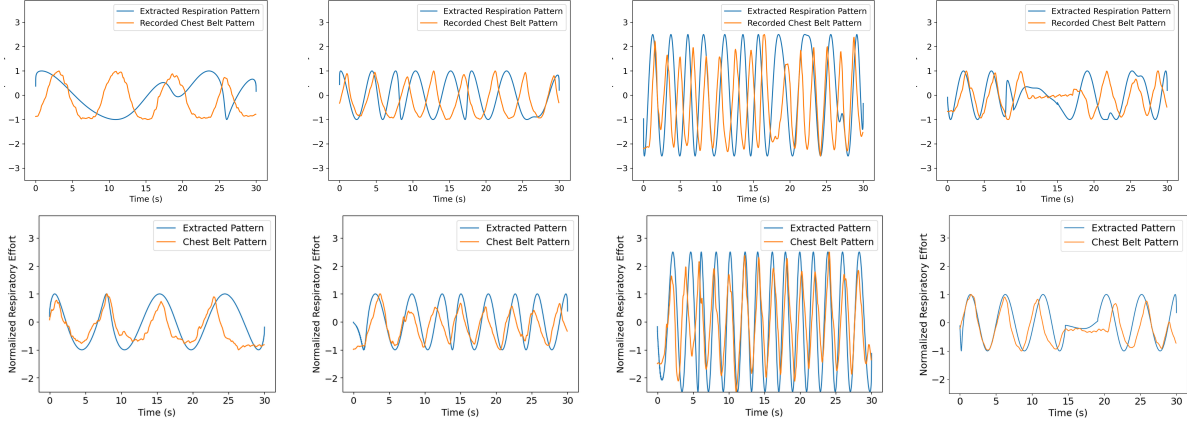
Figure 5. OFDM (top) vs FMCW (bottom): Bradypnea, Eupnea, Kussmaul, Biot.

position for respiratory pattern isolation, and (iii) normalization for amplitude consistency across samples. A total of 200 samples are collected, with 50 samples per respiratory class, resulting in a balanced dataset for training and evaluation.

Table V
PATTERN SIMILARITY UNDER DIFFERENT FMCW-TO-OFDM POWER
RATIOS (2 MHZ SWEEP BANDWIDTH)

MODE	DIFFERENT FMCW POWER RATIOS				
	1.25	1	0.5	0.25	0.1
FMCW	81.6%	**89.2%**	84.4%	86.2%	75.9%
OFDM	79.7%	**83.5%**	84.4%	89.3%	89.5%

C. OFDM and FMCW Pattern Extraction Comparison

To evaluate the consistency of the signal processing pipeline across both modalities, we conducted experiments under two scenarios: static conditions and dynamic conditions with body movement interference.

Static Condition Performance: Under controlled static conditions, both OFDM and FMCW modalities achieve reliable respiration pattern extraction. The extracted signals from FMCW and 5G CSI-phase align well with chest belt references, demonstrating stable and consistent performance despite their differing waveform characteristics. To quantify performance, we compute the similarity between extracted and ground-truth patterns using Fast Dynamic Time Warping (FastDTW). Table V reports the similarity scores under different FMCW-to-OFDM power ratios. A general trend is observed where FMCW similarity decreases with reduced power, while OFDM similarity slightly improves. Based on the power allocation analysis, we consider ratios starting from 1.25 when evaluating trade-offs between sensing and communication. This highlights the importance of selecting a chirp power that balances sensing fidelity with communication quality. For the finalized configuration (ratio = 1), the similarity scores are 89.2% for FMCW and 83.5% for OFDM, indicating that both modalities perform well, with FMCW providing slightly higher fidelity in capturing respiratory dynamics while maintaining reliable communication performance.

Dynamic Condition Performance: When moderate body movements and arm gestures were introduced, the two modalities exhibited distinct robustness. As shown in Fig. 5, OFDM-based CSI-phase extraction suffered from pattern mismatches and increased noise sensitivity. In contrast, FMCW maintained stable and accurate pattern extraction. This difference arises from their sensing mechanisms: OFDM relies on multipath propagation, which is highly susceptible to body-induced channel variations, whereas FMCW leverages direct range measurements, which remain reliable as long as the chest stays within the sensing range.

These experimental observations highlight the key advantage of our composite approach: the FMCW component serves as a robust sensing modality that maintains performance even when the OFDM-based sensing experiences degradation due to environmental interference. This complementary behavior ensures continuous respiration monitoring capability across varying deployment conditions, making the system particularly suitable for practical home healthcare applications where complete environmental control is not feasible.

Table VI
1D-CNN MODEL ARCHITECTURE

LAYER	ACTIVATIONS	INPUT SHAPE	OUTPUT SHAPE
Conv1D	ReLU	(600, 1)	(578, 64)
Conv1D	ReLU	(578, 64)	(556, 64)
GlobalMaxPooling1D	–	(556, 64)	(64)
Flatten	–	(64)	(64)
Dense	ReLU	(64)	(32)
Dense	Softmax	(32)	(4)

D. Respiration Pattern Classification Using 1D-CNN

The extracted respiratory patterns from both sensing modalities are resampled to a uniform length and concatenated to form the input dataset for a one-dimensional Convolutional Neural Network (1D-CNN) model for classification. The consistency achieved through the unified signal processing pipeline across FMCW and 5G modalities allows for the use of a lightweight model architecture without compromising performance. This design choice is particularly advantageous for

ISAC systems, where minimizing computational complexity is critical for real-time implementation. The structure of the 1D-
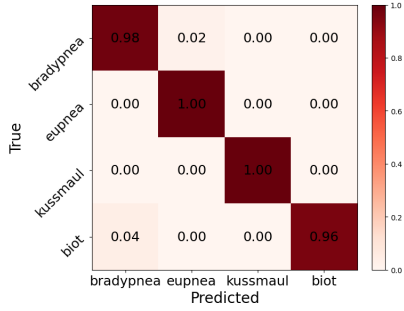

Figure 6. Confusion matrix of the classification model

CNN model is outlined in Table VI. It includes two successive 1D convolutional layers, each with 64 filters and a kernel size of 23, enabling the capture of broad temporal dependencies and distinctive respiratory patterns. This filter configuration balances expressiveness with compactness. A Global Max Pooling layer follows, extracting salient temporal features while enhancing generalization and reducing sensitivity to local input variations. The model achieves an overall classification accuracy of 98%. Fig. 6 shows Eupnea and Kussmaul samples are classified with 100% accuracy. Bradypnea samples achieve 98% accuracy with occasional misclassifications as Eupnea, while Biot samples reach 96% accuracy, with a few misclassifications leaning toward Bradypnea.

VI. CONCLUSION

In this paper, we proposed a practical 28 GHz OFDM–FMCW composite ISAC system that simultaneously supports respiration sensing and communication. By embedding a narrowband FMCW waveform in the OFDM guard band, the design preserved spectral efficiency, avoided complex waveform co-design and additional hardware, and provided resilience to motion interference. To handle real-world interference and bandwidth constraints, we developed a robust signal-processing pipeline integrated with a 1D-CNN classifier. Implemented on an mmWave USRP testbed, the system accurately detected multiple respiratory patterns across varied configurations, achieving up to 98.5% classification accuracy. These findings highlight the feasibility of deploying bandwidth-efficient ISAC systems for contactless health monitoring. Future work will expand data collection to larger and more diverse subject groups, explore NLOS and multi-user scenarios, and investigate additional embedding strategies such as prefix and OFDM idle slot insertion.

ACKNOWLEDGMENT

REFERENCES

[1] Yann Retory, Pauline Niedzialkowski, Carole de Picciotto, Marcel Bonay, and Michel Petitjean. New respiratory inductive plethysmography (RIP) method for evaluating ventilatory adaptation during mild physical activities. *PLoS One*, 11(3):e0151983, March 2016.

[2] K. S. Tan, R. Saatchi, H. Elphick, and D. Burke. Real-time vision based respiration monitoring system. In *2010 7th International Symposium on Communication Systems, Networks & Digital Signal Processing (CSNDSP 2010)*, pages 770–774, 2010. doi: 10.1109/CSNDSP16145.2010.5580316.

[3] Supriya Sathyanarayana, Ravi Kumar Satzoda, Suchitra Sathyanarayana, and Srikanthan Thambipillai. Vision-based patient monitoring: a comprehensive review of algorithms and technologies. *J. Ambient Intell. Humaniz. Comput.*, 9(2):225–251, April 2018.

[4] Yuanhao Cui, Fan Liu, Xiaojun Jing, and Junsheng Mu. Integrating sensing and communications for ubiquitous iot: Applications, trends, and challenges. *IEEE Network*, 35(5):158–167, 2021. doi: 10.1109/MNET.010.2100152.

[5] Jian Liu, Yingying Chen, Yan Wang, Xu Chen, Jerry Cheng, and Jie Yang. Monitoring vital signs and postures during sleep using wifi signals. *IEEE Internet of Things Journal*, 5(3):2071–2084, 2018. doi: 10.1109/JIOT.2018.2822818.

[6] Hao Wang, Daqing Zhang, Junyi Ma, Yasha Wang, Yuxiang Wang, Dan Wu, Tao Gu, and Bing Xie. Human respiration detection with commodity wifi devices: do user location and body orientation matter? In *Proceedings of the 2016 ACM International Joint Conference on Pervasive and Ubiquitous Computing*, UbiComp '16, page 25–36, New York, NY, USA, 2016. Association for Computing Machinery. ISBN 9781450344616. doi: 10.1145/2971648.2971744.

[7] Panagiota Kontou, Souheil Ben Smida, and Dimitris E. Anagnostou. Contactless respiration monitoring using wi-fi and artificial neural network detection method. *IEEE Journal of Biomedical and Health Informatics*, 28(3):1297–1308, March 2024. ISSN 2168-2194. doi: 10.1109/JBHI.2023.3337001. Publisher Copyright: © 2013 IEEE.

[8] Kehan Wu, Renqi Chen, Haiyu Wang, Chenqing Ji, Jiayuan Zhu, and Guang Wu. Passive respiration detection via mmwave communication signal under interference, 2024.

[9] Zhanjun Hao, Yue Wang, Fenfang Li, Guozhen Ding, and Yifei Gao. mmwave-rm: A respiration monitoring and pattern classification system based on mmwave radar. *Sensors*, 24(13), 2024. ISSN 1424-8220. doi: 10.3390/s24134315.

[10] Jiangtao Luo, Kaikai Liu, Yiwen Wang, Lingxia Li, and Zengshan Tian. Respiratory monitoring using millimeter-wave base stations based on ofdm signals. In *2024 IEEE International Instrumentation and Measurement Technology Conference (I2MTC)*, pages 1–5, 2024. doi: 10.1109/I2MTC60896.2024.10560697.

[11] Mostafa Alizadeh, George Shaker, João Carlos Martins De Almeida, Plinio Pelegrini Morita, and Safeddin Safavi-Naeini. Remote monitoring of human vital signs using mm-wave fmcw radar. *IEEE Access*, 7: 54958–54968, 2019. doi: 10.1109/ACCESS.2019.2912956.

[12] Gen Li, Yun Ge, Yiyu Wang, Qingwu Chen, and Gang Wang. Detection of human breathing in non-line-of-sight region by using mmwave fmcw radar. *IEEE Transactions on Instrumentation and Measurement*, 71: 1–11, 2022. doi: 10.1109/TIM.2022.3208266.

[13] Amir Bouziane, Salah Eddine Zegrar, and Hüseyin Arslan. A novel ofdm-fmcw waveform for low-complexity joint sensing and communication. *IEEE Wireless Communications Letters*, 14(2):425–429, 2025. doi: 10.1109/LWC.2024.3506621.

[14] Wenkai Jia, Wen-Qin Wang, Yudian Hou, and Shunsheng Zhang. Integrated communication and localization system with ofdm-chirp waveform. *IEEE Systems Journal*, 14(2):2464–2472, 2020. doi: 10.1109/JSYST.2019.2929254.

[15] Mehmet Mert Şahin and Hüseyin Arslan. Multi-functional coexistence of radar-sensing and communication waveforms. In *2020 IEEE 92nd Vehicular Technology Conference (VTC2020-Fall)*, pages 1–5, 2020. doi: 10.1109/VTC2020-Fall49728.2020.9348582.

[16] Whited L, Hashmi MF, and Graham DD. *Abnormal Respirations*. [Updated 2023 Nov 5], In StatPearls [Internet], 2024.

[17] Guillermo Diaz, Iker Sobron, Iñaki Eizmendi, Iratxe Landa, Johana Coyote, and Manuel Velez. Channel phase processing in wireless networks for human activity recognition. *Internet of Things*, 24:100960, 2023. ISSN 2542-6605. doi: https://doi.org/10.1016/j.iot.2023.100960.